PAPER

Check for updates

Theoretical investigation of thermoelectric properties of methyl blue-based molecular junctions†

Sarah M. S. Al-Mohana,[ab] Hussein N. Najeeb,[c] Rasool M. Al-Utayjawee,[d] Ferydon Babaei[a] and Oday A. Al-Owaedi [ID] *[ce]

Thermoelectric properties of a family of methyl blue-based molecular junctions were theoretically studied using a combination of density functional theory (DFT) methods, and quantum transport theory (QTT). Employing different numbers of amino groups not only proves itself as a powerful strategy for controlling the transport behaviour and lifting the transmission coefficient $T(E)$ from 1.91×10^{-5} to 7.45×10^{-5} with increasing the amino groups from zero to four, but also it enhances the thermoelectric properties of these molecules, since it increases the Seebeck coefficient (S) from 106.8 to 202.4 μV K^{-1} and the electronic figure of merit ($Z_{el}T$) has been raised from 0.15 to 0.35, making these molecules promising candidates for thermoelectric applications.

Introduction

The individual and unique structure of single-molecule materials has made them a goal of many studies that investigate the chemical and physical properties of devices based on single molecules over the past century.[1–5] One of these materials is methyl blue (MB).[6,7] MB is classified as a triaminotriphenyl-methane dye, which is usually recorded as an acid blue 93.[8,9] This kind of dye has attracted wide interest and many applications, such as in textiles, food, rubber, printing, cosmetics, medicine, plastic, concrete, and the paper industry for multiple purposes.[10] In addition, the planarity of sp^2-carbon centers,[11] which form π-orbitals, has granted the MB molecules an attractive functionality as observed by their unique charge transport properties.[12] It is true that the spectroscopy field becomes an attractive source for many researchers[13–20] to explore the spectroscopic properties of single molecules. Consequently, the optical and spectroscopic characteristics of MB molecules have been studied widely, and that encourages researchers to expand their investigation and explore the thermoelectric properties[21–25] of organic molecules, which

significantly improves various applications of single molecule-based molecular junctions ranging from organic electronics[26,27] to molecular sensing,[28,29] light emitting diodes,[30,31] and energy conversion.[32] In this context, the potential of computing and measuring thermoelectric properties of MB molecules will provide a considerable body of information to expand their applications. MB molecule is classified as a small molecule of *ca.* >2 nm, so the coherent electron transport cross the source|MB|drain configuration is depicted as a tunneling process.[33] One of the most important phenomena that governing[34,35] the tunneling mechanism and consequently the properties of molecular nanojunctions is the quantum interference (QI), phenomenon[35] which has been established through a variety of π-conjugated molecules.[36–43] Herein, a combination of density functional theory (DFT) methods,[44,45] quantum transport theory (QTT),[46,47] and an orbital analysis have been used to study the electronic and thermoelectric properties of methyl blue-based molecular junctions. The current work not only explores the effect of number and position of the amine group on thermoelectric properties of MB-based molecular junctions, but also it explores the role of the quantum interference (QI) in determine their transport behaviour.

[a]Department of Physics, Faculty of Science, University of Qom, Qom, 3716146611, Iran

[b]Iraqi Ministry of Education, Babylon Education Directorate, Hilla 51001, Babylon, Iraq

[c]Department of Laser Physics, College of Science for Women, University of Babylon, Hilla 51001, Iraq. E-mail: oday.alowaedi@uobabylon.edu.iq

[d]Iraqi Ministry of Education, Najaf Education Directorate, Najaf, 54001, Iraq

[e]Al-Zahrawi University College, Najaf-Karbala Street, Karbala, 56001, Iraq

† Electronic supplementary information (ESI) available: The theories and all details relevant to the computational methods, as well as it contains the theoretical models of all source|molecule|drain configurations. See DOI: https://doi.org/10.1039/d4ra03574g

Computational methods

The initial optimization of gas phase molecules and isosurfaces calculations were carried out at the B3LYP level of theory[48] with 6-31G** basis set[49,50] using density functional theory (DFT) and time-dependent (TD-DFT)[51] respectively. The geometrical optimization of all gold|MB|gold configurations under investigation in this work was accomplished by the implementation of DFT[45,46] in the SIESTA[45] code, as shown in Fig. 4 and S2 (see

ESI†). The generalized gradient approximation (GGA) of the exchange and correlation functional is used with a double-ζ polarized (DZP) basis set, a real-space grid defined with an equivalent energy cut-off of 250 Ry. The geometry optimization for each structure is performed to the forces smaller than 20 meV Å^{-1}. The mean-field Hamiltonian obtained from the converged DFT calculations was combined with Gollum[52] code. The quantum transport theory (QTT)[53,54] implemented in Gollum have been used to calculate the electronic and thermoelectric properties of all molecular junctions. The optimized molecules have been attached two (111)-directed pyramidal gold electrodes. Each electrode constructed of seven layers of (111)-oriented bulk gold with each layer consisting of 6 × 6 atoms and a layer spacing of 0.235 nm were used to create the molecular junctions. These layers were then further repeated to yield infinitely long gold electrodes carrying current, as shown in Fig. 4, (see ESI† for more details).

Results and discussion

Fig. 1 and Table 1, shows that the molecule length (*l*) of molecule MB-1 equals 1.91 nm, then it decreases to 1.84 nm for molecule MB-2. Molecules MB-3 and MB-4 possess 1.78 and 1.76 nm respectively. The shortest length (1.65 nm) is presented by MB-5. These results could be ascribed to the molecule twisting due to increasing the number of the amino group from 1 to 4. In addition, the HOMO–LUMO gap (H–L gap) of molecules in a gas phase have been fluctuated as well, since it shrinks from 3.5 eV for MB-1 to 2.96 eV for MB-5. The H–L gap of MB-2, MB-3 and MB-4 are 3.47, 3.39 and 3.15 eV respectively.[55,56]

The orbitals distribution and the electronic structure of molecules were investigated and plots of the optimized structures, the highest occupied and lowest unoccupied molecular orbitals (HOMO and LUMO, respectively) are given in Fig. 2. The HOMOs of all molecules display a familiar pattern of π–π interactions along the molecular backbone. The LUMOs are also localized over the molecular backbone and could be described as a π-conjugated system.

In order to explore the impact of connectivity type and to prove the existence of QI in MB molecules, the current investigation performed an orbital analysis, and demonstrated that CQI is dominated on the transport of all molecular junctions, as shown in Fig. 2. Lambert *et al.*[57] have reported an orbital symmetry rule. The magic ratio theory[58] is based on utilising the exact core Green's function, defined by:

$$g(E) = (IE - H)^{-1} \tag{1}$$

In the literature, various approximations to $g(E)$ are discussed, one of which involves the approximation of including only the contributions to $g(E)$ from the HOMO and LUMO. If the amplitudes of the HOMO on sites *a* and *b* are denoted $\psi_a^{E_H}$ and $\psi_b^{E_H}$ and the amplitudes of the LUMO are $\psi_a^{E_L}$ and $\psi_b^{E_L}$, then if the contributions from all other orbitals are ignored, then, a crude approximation to the Green's function $g_{ba}(E)$ is

$$g_{ab}(E) \approx \frac{\psi_a^{(E_H)}\psi_b^{(E_H)}}{E - E_H} + \frac{\psi_a^{(E_L)}\psi_b^{(E_L)}}{E - E_L} \tag{2}$$

where E_H and E_L are the energies of the HOMO and LUMO respectively. If the HOMO product $\psi_b^{(E_H)}\psi_a^{(E_H)}$ has the same sign as the LUMO product $\psi_b^{(E_L)}\psi_a^{(E_L)}$ then the right-hand side of eqn
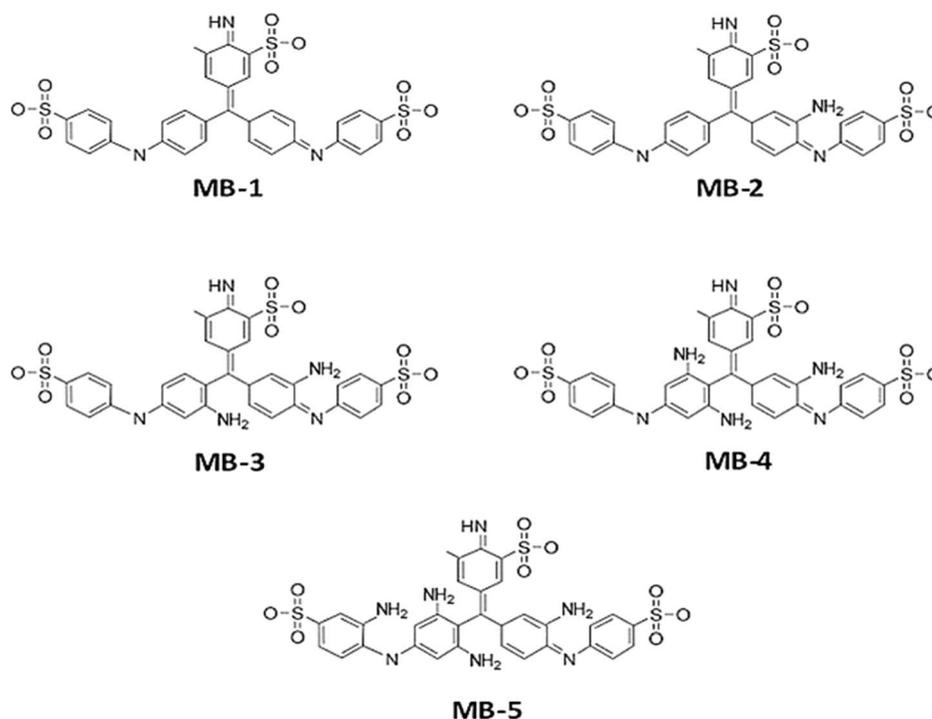

Fig. 1 Schematic illustration of MB molecules.

Table 1 Number of amino group (N); molecule length (l); molecular length (d = Au⋯Au); theoretical electrode separation ($Z = d_{\text{Au–Au}} - 0.25$), where 0.25 nm is the calculated centre-to-centre distance of the apex atoms of the two opposing gold electrodes when conductance = G_0 in the absence 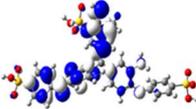of the molecule, G_0 is the conductance quantum; highest occupied molecular orbitals (HOMO); lowest unoccupied molecular orbitals (LUMO); HOMO–LUMO gap (H–L gap); A is the absorption intensity; $^A\lambda_{\text{Max}}$ is the maximum absorption wavelength; E is the emission intensity; $^E\lambda_{\text{Max}}$ is the maximum emission wavelength; f_{em} is emission oscillator strength; SS is the Stokes shift
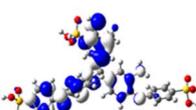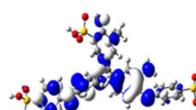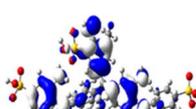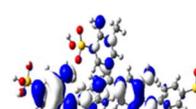
Molecule	N	l (nm)	d (nm)	Z (nm)	HOMO (eV)	LUMO (eV)	H–L gap (eV)	A (a.u.)	$^A\lambda_{\text{Max}}$ (nm)	E (a.u.)	$^E\lambda_{\text{Max}}$ (nm)	f_{em}	SS (nm)
MB-1	0	1.91	2.155	1.905	5.58	2.08	3.5	65.02	816	11 319	944	0.203	128
MB-2	1	1.84	2.085	1.835	5.6	2.13	3.47	54.92	800	9201	900	0.217	100
MB-3	2	1.78	2.025	1.775	5.38	1.99	3.39	46.99	750	8247	890	0.171	140
MB-4	3	1.76	2.005	1.755	5.05	1.9	3.15	80.56	800	13 433	900	0.33	100
MB-5	4	1.65	1.895	1.645	4.94	1.98	2.96	72.06	848	13 796	1016	0.37	168

(2) will vanish at some energy E in the range $E_{\text{H}} \nleqq E \nleqq E_{\text{L}}$. That is for some energy E within the HOMO–LUMO gap. In this case, one can say that the HOMO and the LUMO interfere destructively. On the other hand, if the HOMO and LUMO products have opposite signs then the right hand side of eqn (2) will not vanish within the HOMO–LUMO gap and one can say
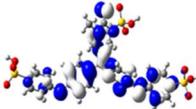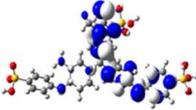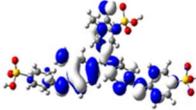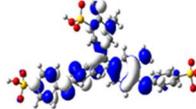
Fig. 2 The highest occupied and lowest unoccupied molecular orbitals (HOMOs and LUMOs) (isosurfaces ± 0.02 (e bohr^{-3})$^{1/2}$), white part is a positive sign, blue part is a negative sign. $a_{\text{H}} \times a_{\text{L}}$ is the multiplication of the HOMO and LUMO amplitudes. As an example, HOMO and LUMO for MB-5 molecule possess different signs, then the multiplication of molecular orbitals amplitudes ($a_{\text{H}} \times a_{\text{L}}$) is a negative sign and the molecule exhibits a constructive quantum interference (CQI).

that the HOMO and LUMO interfere constructively within the gap, (they could of course interfere destructively at some other energy E outside the gap). When the right-hand side of eqn (2) vanishes, the main contribution to $g_{ba}(E)$ comes from all other orbitals, so in general eqn (2) could be a poor approximation. One exception to this occurs when the lattice is bipartite, because the Coulson–Rushbrooke (CR) theorem[59] tells us that if a and b are both even or both odd, then the orbital products on opposite sides of eqn (3) and (4) have the same sign. Consequently, the HOMO and LUMO interfere destructively, while all other pairs of orbitals interfere destructively, leading to the trivial zeros in the magic number table,[58] for which $g_{ba}(0) = 0$.

$$\psi_a^{(E_n)}\psi_b^{(E_n)} = \psi_a^{(-E_n)}\psi_b^{(-E_n)} \tag{3}$$

$$\phi_b^{(E_n)}\phi_b^{(E_n)} = \phi_b^{(-E_n)}\phi_b^{(-E_n)} \tag{4}$$

where $\pm E_n$ are eigenvalues come in $\pm$ pairs and the eigenstate belonging to $-E_n$ is related to the eigenstate belonging to E_n. Obviously, this exact cancellation is a property of bipartite lattices only, but based on its success for bipartite lattices, one might suppose that eqn (2) is a reasonable approximation, for other lattices. Nevertheless, as pointed out by Yoshizawa *et al.*,[60-63] since orbitals such as those in Fig. 2 are often available from DFT calculations, it can be helpful to examine the question of whether or not the HOMO and LUMO (or indeed any other pair of orbitals) interfere destructively or constructively, by examining the colours of orbitals. This is simplified by writing eqn (2) in the form

$$g_{ab}(E) \approx \frac{a_H}{E - E_H} + \frac{a_L}{E - E_L} \tag{5}$$

where $a_H = \psi_a^{(E_H)}\psi_b^{(E_H)}$ and $a_L = \psi_a^{(E_L)}\psi_b^{(E_L)}$. If the HOMO product a_H has the same sign as the LUMO product a_L then the right-hand side of eqn (5) will vanish for some energy E in the range $E_H \nleqq E \nleqq E_L$. In other words, the HOMO and LUMO will interfere destructively at some energy within the HOMO–LUMO gap. However this does not mean that the exact $g_{ba}(E)$ will vanish. Indeed, if the right hand side of (5) vanishes, then the contributions from all other orbitals become the dominant terms.[64] Nevertheless, this is an appealing method of identifying QI effects in molecules and describing their qualitative features.[65]

The distinctive properties of MB molecules including for example their spectroscopic properties, especially the absorption and emission spectra, have become the subject of the increased interest for many studies.[66] Interestingly, the UV/visible absorption and emission spectra showed asymmetric peaks, since the range of the absorption spectra is extend from 750 to 848 nm, as shown in Table 1, and the emission spectra is ranging from 890 to 1016 nm. These results could be interpreted in terms of strain and twisting effects, which are critical qualities that endows molecules atypical spectroscopic properties and reactivity. The inherent strain of the molecule increases with increasing of the amino group number and consequently leads to twisting, which in turn changes the structural and spectroscopic properties. The methyl blue molecule (MB-1) do

not possess an amino group. Thus, this molecule is expect to exhibit a largest HOMO–LUMO gap, as shown in Table 1. These results are consistent with the results of references.[67,68] Furthermore, Fig. 3 and Table 1 show that the Stokes shift of these molecules is ranging from 100 to 168 nm. Therefore, these results may introduce MB molecules as promising candidates for the encryption and medical applications.[69,70] On the other hand, the most important parameters in optoelectronics applications is the emission oscillator strength (f_{em}).[71] Theoretically, for a given PL material, f_{em} is directly proportional to the emission cross section (σ_{em}) and it is given by:[72]

$$\sigma_{em}(\nu) = \frac{e^2}{4\varepsilon_0 m_e c_0 n_F} g(\nu)f_{em} \tag{6}$$

where e is the electron charge, ε_0 is the vacuum permittivity, m_e is the mass of electron, c_0 is the speed of light, n_F is the refractive index of the gain material, ν is the frequency of the corresponding emission, and $g(\nu)$ is the normalized line shape function with $\int g(\nu) \, d\nu = 1$. The emission oscillator strength (f_{em}) of MB molecules is ranging from 0.17 to 0.37, as shown in Table 1.

In this work $T(E)$ has been calculated by attach the optimized molecules with two (111)-directed gold electrodes, as shown in Fig. 4. From these molecular junctions the electronic and thermoelectric properties were calculated using Gollum code.[52] The transmission coefficient according to Landauer–Büttiker[73] formalism is given by:

$$T(E) = T_r\{\Gamma_R(E)G^R(E)\Gamma_L(E)G^{R\dagger}(E)\} \tag{7}$$

where

$$\Gamma_{L,R}(E) = i(\Sigma_{L,R}(E) - \Sigma_{L,R}^\dagger(E)) \tag{8}$$

where $\Gamma_{L,R}$ describes the level broadening due to the coupling between left (L) and right (R) electrodes and the central scattering region, $\Sigma_{L,R}(E)$ are the retarded self-energies associated with this coupling.

$$G^R = (EX - \hat{H} - \Sigma_L - \Sigma_R)^{-1} \tag{9}$$

where G^R is the retarded Green's function, $\hat{H}$ is the Hamiltonian and X is the overlap matrix. The transport properties is then calculated using the Landauer formula:

$$G = G_0 \int dE T(E)(-\partial f(E, T)/\partial E) \tag{10}$$

where $G_0 = 2e^2/h$ is the conductance quantum, $f(E) = (1 + \exp((E - E_F)/k_BT))^{-1}$ is the Fermi–Dirac distribution function, T is the temperature and $k_B = 8.6 \times 10^{-5}$ eV K^{-1} is Boltzmann's constant.

Fig. 4 and 5 show that the molecules bind to gold electrodes through sulfonyl groups as anchor groups. It is true that the binding between sulfonyl groups and electrodes is uncommon due to the formation of hypervalent five-coordinate sulfur atoms. However, the results of Fig. 5 suggest considerable values of the binding energy, which are consistent with the outcomes of H. Quan *et al.*,[74] since they reported that the
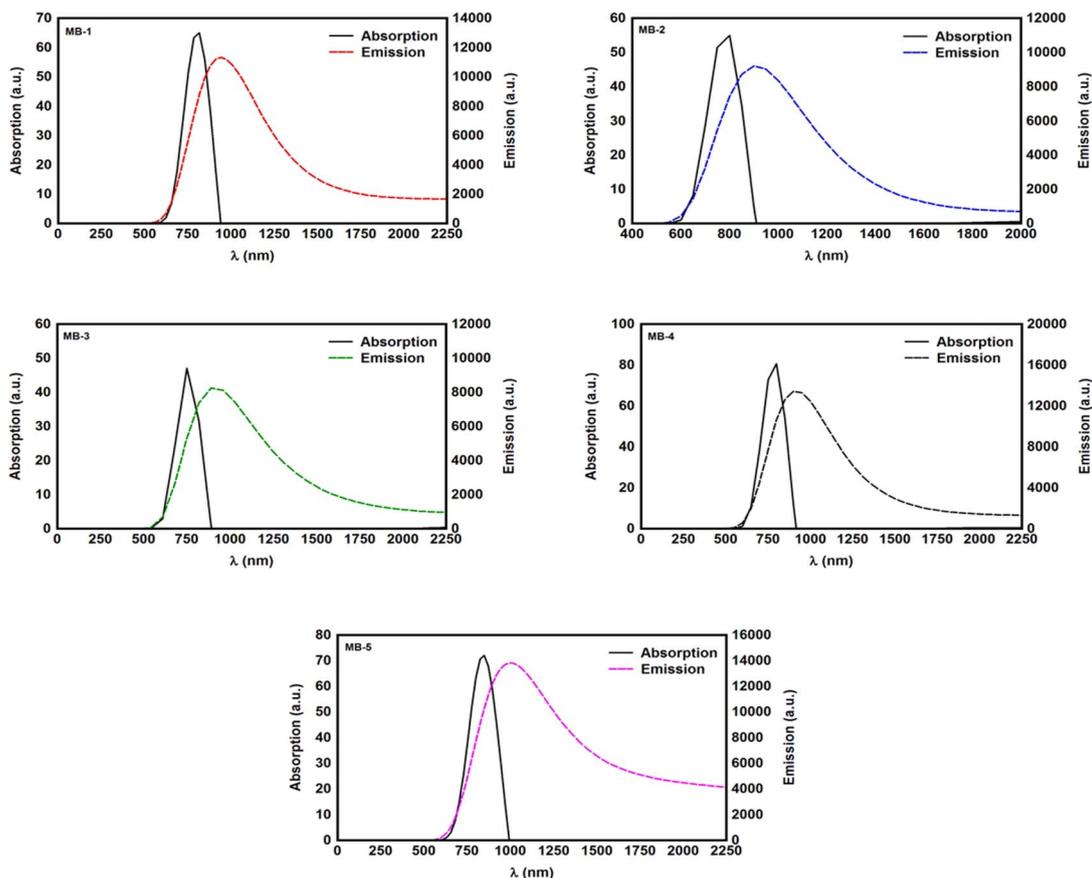
Fig. 3 UV/Vis absorption spectra (solid curves) and emission spectra (dashed curves) for all molecules.
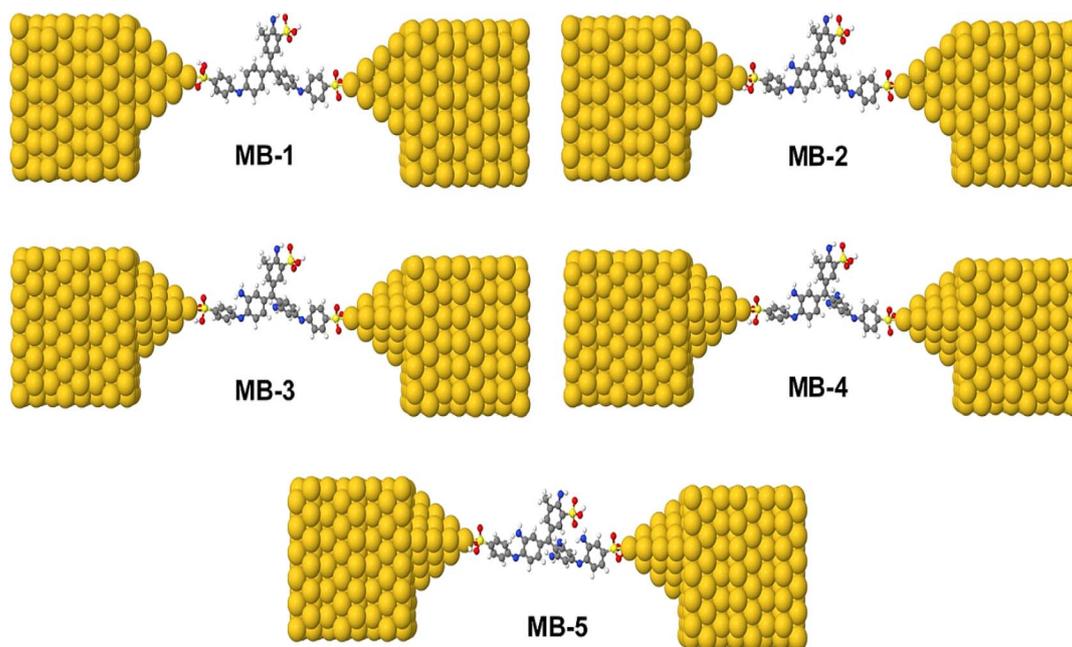
Fig. 4 Theoretical models of optimized molecular junctions.

presence of strong electron-withdrawing groups on benzene sulfonyl 5-FU greatly enhanced the binding selectivity.[75,76] To perform accurate calculations of the transmission coefficient for the molecular junctions with sulfonyl-anchor groups, the binding energies were computed using eqn (11), for a range of diverse molecular direction within the junction (know by the

Fig. 5 (a) The binding energy as a function of the angle (Θ) between anchor group and gold electrode; (b) the binding energy as a function of the molecular junction displacement (D).

angle Θ, $\angle C_{ipso}$–S–Au) as shown in Fig. 5. The maximum binding energies arranged between -0.73 and -0.74 eV for the angles from $140°$ to $180°$, as show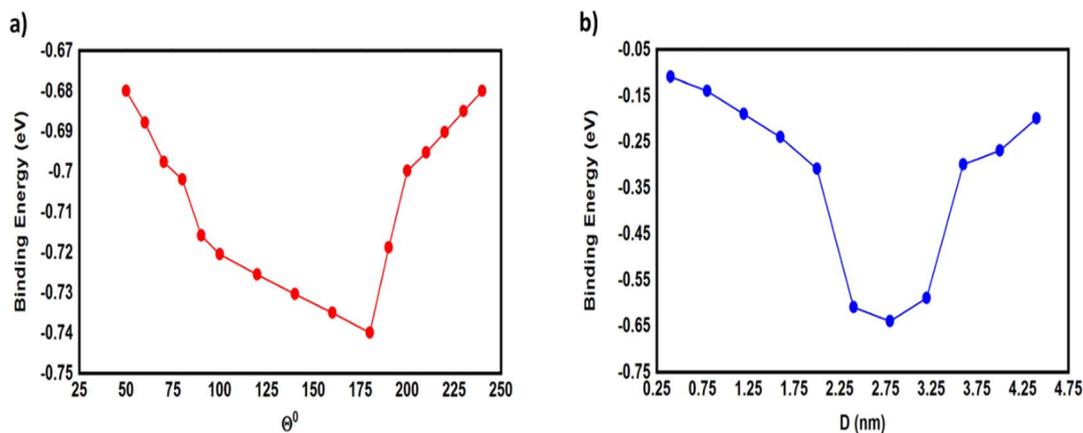n in Fig. 5a. Allowing for room-temperature thermal fluctuations of (~ 25 meV), this proposes that the optimal conformation is within the angle Θ equals $180°$.

$$\Delta E(ab) = E_{ab} - (E_a^{ab} + E_b^{ab}) \qquad (11)$$

The molecular systems are denoted a and b. The total energy of the combined a and b systems is E_{ab}, while the total energies of isolated systems a and b are E_a and E_b respectively with keeping identical basis sets for the three energies. ΔE_{ab} is the binding energy (BE) between anchor groups and gold electrode.

To gain further insight into the evolution of the binding energy (BE) upon stretching, and to obtain a robust value of the BE between anchor group and gold electrode, we calculated the most probable energies at each relative displacement position. The most-probable absolute displacements (D) in an experimental molecular junction formed between a gold STM tip and an Au(111) surface are obtained by adding the snapback distance $\Delta D_{corr} = (0.5 \pm 0.1$ nm$)$[77–79] to the relative displacement $D = \Delta D + \Delta D_{corr}$. Fig. 5b shows that the highest values of BE ranging between -0.59 and -0.64 eV for the displacements 2.4, 2.8 and 3.2 nm, and the maximum binding energy (-0.64 eV) for the displacement of 2.8 nm.

Fig. 6 shows the transmission coefficient $T(E)$,[80] of source|molecule|drain molecular junctions. The signature of a constructive quantum interference (CQI) is clear for all molecules, which leads to high $T(E)$ values, as shown in Fig. 6 and Table 2. These outcomes are ascribed to the para connectivity[81–86] between phenyl rings. The order of $T(E)$ is $T_{MB-5} > T_{MB-4} > T_{MB-3} > T_{MB-2} > T_{MB-1}$, as shown in Table 2. For all cases, the Fermi level (E_F–E_F^{DFT}) lies within the HOMO–LUMO gap towards the HOMO resonance, which remarks a HOMO-dominated transport mechanism.

These consequences are consistent with the results of references.[87,88] The results could be understood in terms of the
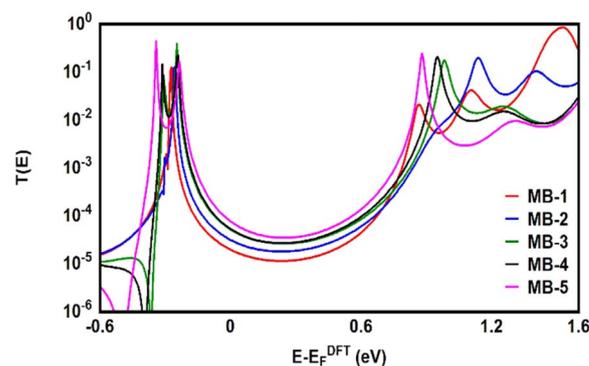

Fig. 6 Transmission coefficient $T(E)$ as a function of electrons energy for all molecules.

inherent strain, which resulted to the molecular twisting which in turn decreased the tunnelling distance (l) and consequently increasing $T(E)$, according to eqn (12).

$$T(E) \propto e^{-\beta l} \qquad (12)$$

where, $T(E)$ is the transmission coefficient, β is the electronic decay constant and l is the tunnelling distance. In addition, the molecule length of all molecules is smaller than 2 nm, which is consistent with a dominant contribution from coherent tunneling mechanism.[89–93] The rectangular tunnel barrier model[94] states that the electrical conductance through a single molecule (barrier) decreases exponentially with the length of the barrier, according to eqn (12).

To gain more knowledge of electronic transitions, and the effect of different numbers of an amino group on electron transport, Mulliken population[95] was computed to characterize the electronic charge distribution, and the number of electrons transferred from the molecule to the electrodes, as shown in Fig. 7 and Table 2. There is an important result, which is the number of calculated electrons transfer from molecule to the electrodes (Γ) ranges from *ca.* 1.3 electron for MB-1 molecule to 2.6 electron for MB-5. A partial charge transfer has been

Table 2 Number of transfer electrons ($\Gamma = e_M - e_J$), where e_M is the number of electrons on the molecule in a gas phase, e_J is the number of electrons on the molecule in a junction; transmission coefficient $T(E)$; molecule length (l = SS); highest occupied molecular orbitals of the molecules in a junction (^{J}HOMO); lowest unoccupied molecular orbitals of the molecules in a junction (^{J}LUMO); HOMO–LUMO gap (^{J}H–L gap) of the molecules in a junction

| Molecule	Γ	$T(E)$	^{J}HOMO (eV)	^{J}LUMO (eV)	^{J}H–L gap (eV)
MB-1	1.3	1.91×10^{-5}	0.27	0.86	1.13
MB-2	1.7	3.06×10^{-5}	0.26	1.13	1.39
MB-3	2.1	5.02×10^{-5}	0.25	0.98	1.23
MB-4	2.3	5.17×10^{-5}	0.31	0.95	1.26
MB-5	2.6	7.45×10^{-5}	0.34	0.88	1.22

observed,[96] which is consistent with the energetic location of frontier molecular orbitals as discussed by Thygesen et al.[97] Now, by comparing the number of Γ from molecule MB-1 relative to that of molecule MB-5. An increase of the number of amino groups from zero to four increases the electron donor atoms (nitrogen atoms), which rises Γ from 1.3 to 2.6 electron. In addition, the effects of the inherent strain and molecular twisting decrease the molecule length from 1.91 nm for MB-1 to 1.65 nm for MB-5. The latter contributes with CQI in lifting the transmission coefficient from 1.91×10^{-5} to 7.45×10^{-5} for MB-1 and MB-5 respectively, as shown in Fig. 7.

The slope of $T(E)$ determines the Seebeck coefficient (S) and electronic figure of merit ($Z_{el}T$), which are given by:

$$S \approx -L|e|T\left(\frac{d\ln T(E)}{dE}\right)_{E=E_F} \tag{13}$$

where L is the Lorenz number $L = \left(\frac{k_B}{e}\right)^2 \frac{\pi^2}{3} = 2.44 \times 10^{-8}$ W Ω K^{-2}. In other words, S is proportional to the negative of the slope of ln $T(E)$, evaluated at the Fermi energy. Based on Seebeck coefficient, the power factor was calculated by:

$$P = GS^2T \tag{14}$$
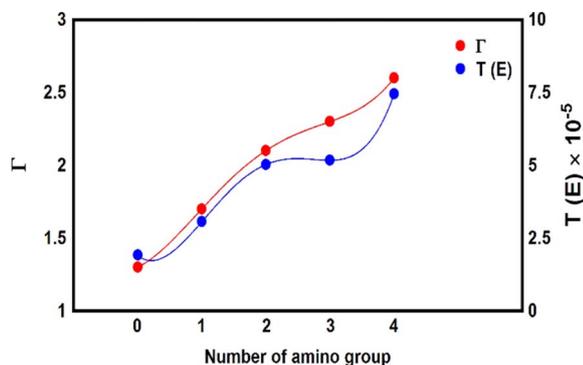
Fig. 7 The number of transferred electrons from molecule to electrodes (Γ) for all molecules.

where T is the temperature $T = 300$ K, G is the electrical conductance and S is the Seebeck coefficient. The purely electronic figure of merit ($Z_{el}T$) is given by:[98,99]

$$Z_{el}T = \frac{S^2G}{k_{el}}T = \frac{S^2}{L} \tag{15}$$

where k_{el} is the electron thermal conductance. According to previous studies,[98,99] the figure of merit in this work has been calculated only based on a purely electronic contribution, as shown in eqn (15).

It is well known that the performance of thermoelectric materials is characterized by an efficient conversion of an input heat to the electricity.[100,101] In this context, the enhancement of power factor (P) and electronic figure of merit ($Z_{el}T$), which are depend on the Seebeck coefficient (S) is important. Fig. 8a and b and Table 3 show the highest values of S and $Z_{el}T$ (202.4 μV K^{-1} and 0.36 respectively) have been exhibited by molecule MB-3. In contrast, molecule MB-1 presented the lowest values of these parameters (106.8 μV K^{-1}, and 0.15). In addition, molecules MB-4 and MB-5 introduce high S and $Z_{el}T$, as shown in Table 3. These results not only demonstrated the important role of the existence and number of amino group in improvement S and $Z_{el}T$, but also established a crucial role of the inherent strain in MB molecules, which controls the transport behaviour and improves the thermoelectric properties of these molecules. Furthermore, the competition between electrical conductance and Seebeck coefficient according to eqn (14) led to the power factor order of $P_{MB-5} > P_{MB-3} > P_{MB-4} > P_{MB-2} > P_{MB-1}$. In light of the aforementioned results, these molecules could be considered as promise candidates for thermoelectric applications.

The values of the transmission coefficient $T(E)$, Seebeck coefficient (S) and electronic figure of merit ($Z_{el}T$) are found to be higher when the contact Fermi energies are close to the middle of the HOMO–LUMO gap and increases as Fermi energies approach resonance with the highest occupied molecular orbitals (HOMO). In somewhat, these results are consistent with an investigation of David C. Milan et al.,[93] since they reported that the existent of different solvent environments affect both the molecular junction conductance and the attenuation factors. These properties are depend in a very sensitive manner on the position of the contact Fermi energies within in the HOMO–LUMO gap.

Fang Chen et al.[102] have studied the effect of different anchoring groups on the conductance of single molecules using alkanes terminated with dithiol, diamine, and dicarboxylic-acid groups as a model system. They observed that the conductance is highly sensitive to the anchoring group type. They interpreted these observations in terms of the different electronic couplings between the molecules and the electrodes and alignments of the molecular energy levels relative to the Fermi energy level of the electrodes introduced by different anchoring groups. Moreover, they mentioned that the conductance of molecules terminated with diamine and dicarboxylic-acid groups, is sensitive to pH due to protonation and deprotonation of the anchoring groups.

Fig. 8c and d and Table 3 present the current–voltage (I–V) characteristics of all molecular junctions, which are limited to
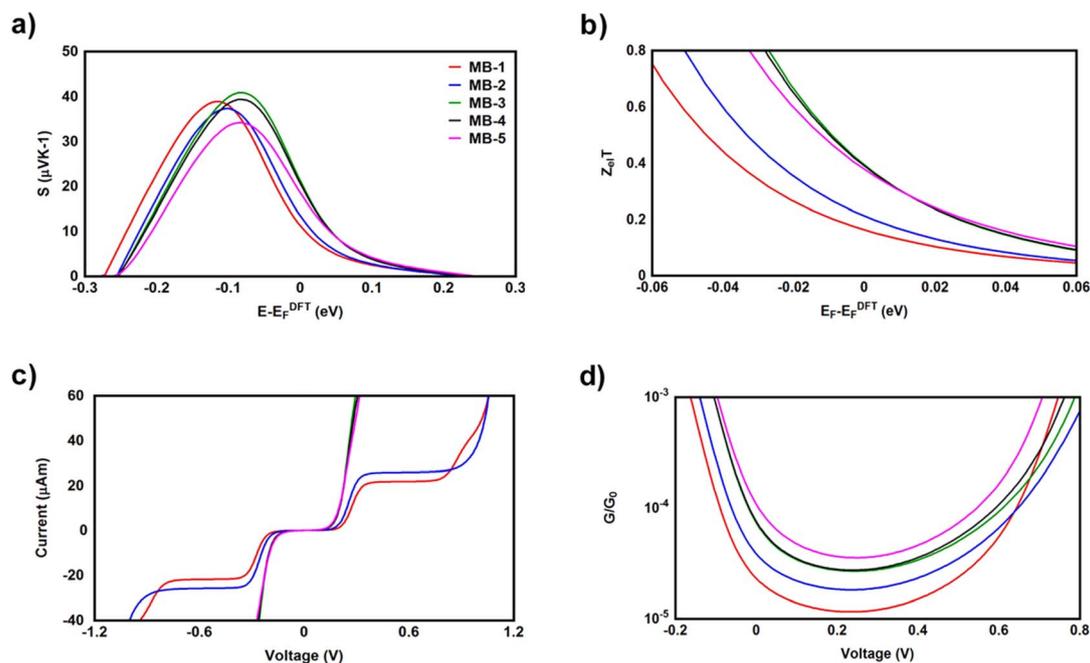
Fig. 8 (a) Seebeck coefficient (S); (b) electronic figure of merit ($Z_{el}T$); (c) current–voltage characteristics; (d) electrical conductance (G/G_0) as a function of applied voltage for all molecular junctions.

Table 3 Seebeck coefficient (S); electronic figure of merit ($Z_{el}T$); power factor (P); threshold voltage (V_{th}); Peltier coefficient (Π) for all molecular junctions

Molecule	S (μV K^{-1})	P (W K^{-1} × 10^{-18})	$Z_{el}T$	V_{th} (V)	Π (J C^{-1})
MB-1	106.8	16.9	0.15	0.23	0.034
MB-2	127.6	38.6	0.19	0.22	0.040
MB-3	202.4	159.5	0.36	0.18	0.064
MB-4	196.9	155.6	0.36	0.19	0.062
MB-5	178.3	183	0.35	0.18	0.056

the first and third quadrants of the I–V plane crossing the origin. Therefore, they are classified as components consume the electric power, and here the importance of the threshold voltage (V_{th}) value appears. The values of V_{th} are ranging from 0.18 to 0.23 V, which makes these molecules promising candidates for the electronic applications. Moreover, I–V characteristics of MB-3, MB-4 and MB-5 molecular junctions exhibited a semiconductor behaviour, while MB-1 and MB-2 show a quantum staircase structure in the conductance. Obviously, as the voltage increases, the density of electrons also increases, which leads to an increase in the number of occupied subbands. The dependence conductance in this case is a set of plateaus separated by steps of height $2e^2/h$: a stepwise change in the conductance of MB-1 and MB-2 molecules channels occurs each time the Fermi level coincides with one of the subbands. Hence, the quantum staircase behaviour could be attributed to the adiabatic transparency of spin-nondegenerate subbands of these molecules.[65,103]

The Peltier coefficient refers to the reversible absorption or liberation of heat at the junction of two materials depending on

the direction of a current, I, flowing through the junction. One main component of the heat exchange at the junction of two materials is the irreversible heat dissipation (Joule heating) which has the form $QJ = IR^2$, where R is the junction resistance.[104] Joule heating has been recently observed down to atomic-scale.[105] Another component is the reversible heat exchange due to Peltier effect which has the form $QP = \Pi I$, where Π is the Peltier coefficient. One important aspect of the Peltier effect is that the direction of the heat exchange at the junction (that is, heating or cooling) can be controlled *via* switching the current direction. Herein, Fig. 9 and Table 3 show that Peltier values are impalpable at low temperatures, and then begin to increase gradually as temperatures rise. Over a wide range of temperatures, starting from the room temperature (300 K) upwards, Peltier values were steadily increasing. This result
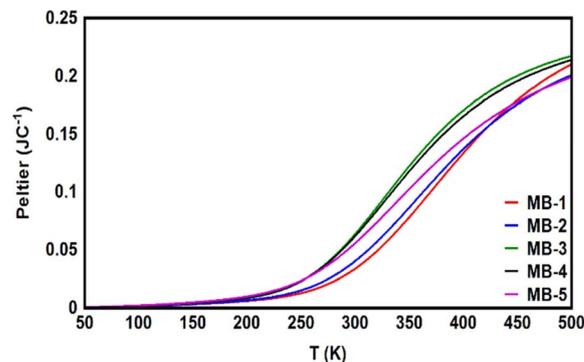

Fig. 9 Peltier coefficient as a function of the temperature for all molecules.

is consistent with the current–voltage characteristic results in Fig. 8. Remarkably, molecule MB-3 presented the highest value (0.064 JC^{-1}), while molecule MB-1 shows the lowest Peltier value (0.034 J C^{-1}). The overall order of values was $\Pi_{\text{MB-3}} > \Pi_{\text{MB-4}} > \Pi_{\text{MB-5}} > \Pi_{\text{MB-2}} > \Pi_{\text{MB-1}}$.

Conclusions

In conclusions, the existent of amino groups leads to increase the inherent strain, and molecular twisting which decreases the molecule length, and the latter along with the effect of CQI rises $T(E)$. The high calculated values of S predicate that MB molecules could be promise candidates for thermoelectric applications. The semiconductor and the quantum staircase behaviors as well as the low threshold voltages of MB molecules suggest that these structures could be suitable compounds for electronic applications. Furthermore, the values of Stokes shift (SS) predicate that MB molecules could be appropriate structures for encryption and medical applications. Please refer to the ESI† for the theories and all details relevant to the computational methods.[106–115]

Data availability

The data is available at the manuscript and ESI.†

Author contributions

Sarah M. S. Al-Mohana: conceptualization, validation, formal, analysis, investigation, writing – original draft, visualization, Hussein N. Najeeb: software, formal analysis. Rasool M. Al-Utayjawee: investigation. Ferydon Babaei: supervision, investigation, analysis, conceptualization, writing – review & editing. Oday A. Al-Owaedi: software, formal analysis, writing – review & editing.

Conflicts of interest

The authors declare no competing financial interest.

Acknowledgements

Notes and references

1 L. Jacob, G. Alessio, P. Alessandro and S. C. Gemma, *ACS Nano*, 2013, **7**, 9183–9194.

2 A. Q. David, S. C. Gemma, G. H. Randall, H. Thorsten, W. R. Michael, V. P. Richard and R. A. Mark, *J. Phys. Chem. C*, 2008, **112**, 16991–16998.

3 H. Bing, L. Xu, Y. Ying, H. Ze-Wen, Z. Ju-Fang, P. Lin-Qi, S. Yong, L. Jian-Feng, Z. Xiao-Shun, C. Jing-Zhe, J. Shan and M. Bing-Wei, *J. Am. Chem. Soc.*, 2018, **140**, 17685–17690.

4 A. Renad, H. Songjun, W. Qingqing, L. Zitong, H. Wenjing and C. J. Lambert, *ACS Sens.*, 2021, **6**, 470–476.

5 O. A. Al-Owaedi, S. Bock, D. C. Milan, M. Oerthel, M. S. Inkpen, D. S. Yufit, A. N. Sobolev, N. J. Long, T. Albrecht, S. J. Higgins, M. R. Bryce, R. J. Nichols, C. J. Lambert and P. J. Low, *Nanoscale*, 2017, **9**, 9902–9912.

6 A. Fernández-Pérez and G. Marbán, *ACS Omega*, 2020, **5**, 29801–29815.

7 T. B. de Queiroz, E. R. de Figueroa, M. D. Coutinho-Neto, C. D. Maciel, E. Tapavicza, Z. Hashemi and L. Leppert, *J. Chem. Phys.*, 2021, **154**, 044106.

8 K. A. S. Schulte, H. J and J. K. Sugden, *Dyes Pigm.*, 1997, **34**, 159–167.

9 Y. Feng, Y. Li, M. Xu, S. Liua and J. Yao, *RSC Adv.*, 2016, **6**, 109608.

10 M. Hassan, M. D. Al-Ahmadi and M. Mosaid, *Arabian J. Chem.*, 2015, **8**, 72–77.

11 Y. Shigeru and K. Eiichi, *J. Synth. Org. Chem., Jpn.*, 2019, **77**, 1147–1158.

12 S. S. Hemdan, *J. Fluoresc.*, 2023, **33**, 2489–2502.

13 W. E. Moerner and T. Basché, *Angew. Chem., Int. Ed.*, 1993, **54**, 105–537.

14 W. E. Moerner, *Science*, 1994, **265**, 46–53.

15 M. Orrit, J. Bernard, R. Brown and B. Lounis, *Prog. Opt.*, 1996, **35**, 61–144.

16 T. Plakhotnik, E. A. Donley and U. P. Wild, *Annu. Rev. Phys. Chem.*, 1997, **48**, 181–212.

17 S. Nie and R. N. Zare, *Annu. Rev. Biophys. Biomol. Struct.*, 1997, **26**, 567–596.

18 W. E. Moerner, *Science*, 1999, **283**, 1670–1676.

19 P. Tinnefeld and M. Sauer, *Angew. Chem., Int. Ed.*, 2005, **44**, 2642–2671.

20 P. V. Cornish and T. Ha, *ACS Chem. Biol.*, 2007, **2**, 53–61.

21 L. Fan, X. Su, H. Zhu, H. Liu, S. Lou, Y. Shi and S. Yan, *Adv. Mater. Interfaces*, 2023, **10**, 2202207.

22 O. A. Al-Owaedi, D. C. Milan, M. Oerthel, S. Bock, D. S. Yufit, J. A. K. Howard, S. J. Higgins, R. J. Nichols, C. J. Lambert, M. R. Bryce and P. J. Low, *Organometallics*, 2016, **35**, 2944–2954.

23 R. S. Akbarabadi, R. H. Soleimani and B. M. Tagani, *Sci. Rep.*, 2021, **11**, 8958.

24 S. V. Aradhya and L. Venkataraman, *Nanotechnology*, 2013, **8**, 399–410.

25 G. Sedghi, L. J. Esdaile, H. L. Anderson, V. M. García-Suárez, C. J. Lambert, S. Martin, D. Bethell, S. J. Higgins and R. J. Nichols, *Nat. Nanotechnol.*, 2011, **6**, 517–523.

26 M. Ball, Y. Zhong, B. Fowler, B. Zhang, P. Li, G. Etkin, D. W. Paley, J. Decatur, A. K. Dalsania, H. Li, S. Xiao, F. Ng, M. L. Steigerwald and C. Nuckolls, *J. Am. Chem. Soc.*, 2016, **138**, 12861–12867.

27 E. Kayahara, L. Sun, H. Onishi, K. Suzuki, T. Fukushima, A. Sawada, H. Kaji and S. Yamago, *J. Am. Chem. Soc.*, 2017, **139**, 18480–18483.

28 T. Iwamoto, Y. Watanabe, T. Sadahiro, T. Haino and S. Yamago, *Angew. Chem., Int. Ed.*, 2011, **50**, 8342–8344.

29 P. Li, T. J. Sisto, E. R. Darzi and R. Jasti, *Org. Lett.*, 2014, **16**, 182–185.

30 M. Naher, D. C. Milan, O. A. Al-Owaedi, I. J. Planje, S. Bock, J. Hurtado-Gallego, P. Bastante, Z. M. A. Dawood, L. Rincón-García, G. Rubio-Bollinger, S. J. Higgins, N. Agraït, C. J. Lambert, R. J. Nichols and P. J. Low, *J. Am. Chem. Soc.*, 2021, **143**(10), 3817–3829.

31 D. Z. Manrique, C. Huang, M. Baghernejad, X. Zhao, O. A. Al-Owaedi, H. Sadeghi, V. Kaliginedi, W. Hong, M. Gulcur, T. Wandlowski, M. R. Bryce and C. J. Lambert, *Nat. Commun.*, 2015, **6**, 6389.

32 H. Kirchberg and A. Nitzan, *J. Chem. Phys.*, 2022, **156**, 094306.

33 T. A. Su, M. Neupane, M. L. Steigerwald, L. Venkataraman and C. Nuckolls, *Nat. Rev. Mater.*, 2016, **1**, 16002.

34 M. Baghernejad, Y. Yang, O. A. Al-Owaedi, Y. Aeschi, B. Zeng, Z. M. Dawood, X. Li, J. Liu, J. Shi, D. Silvio, S. Liu, W. Hong and C. J. Lambert, *Chem.–Eur. J.*, 2020, **26**, 5264–5269.

35 P. Sautet and C. Joachim, *Chem. Phys. Lett.*, 1988, **153**, 511–516.

36 M. Mayor, H. B. Weber, J. Reichert, M. Elbing, C. von Hänisch, D. Beckmann and M. Fischer, *Angew. Chem., Int. Ed.*, 2003, **42**, 5834–5838.

37 M. Taniguchi, M. Tsutsui, R. Mogi, T. Sugawara, Y. Tsuji, K. Yoshizawa and T. Kawai, *J. Am. Chem. Soc.*, 2011, **133**, 11426–11429.

38 C. M. Guédon, H. Valkenier, T. Markussen, K. S. Thygesen, J. C. Hummelen and S. J. van der Molen, *Nat. Nanotechnol.*, 2012, **7**, 305.

39 S. V. Aradhya, J. S. Meisner, M. Krikorian, S. Ahn, R. Parameswaran, M. L. Steigerwald, C. Nuckolls and L. Venkataraman, *Nano Lett.*, 2012, **12**, 1643–1647.

40 C. R. Arroyo, S. Tarkuc, R. Frisenda, J. S. Seldenthuis, C. H. M. Woerde, R. Eelkema, F. C. Grozema and H. S. J. van der Zant, *Angew. Chem., Int. Ed.*, 2013, **52**, 3152–3155.

41 Y. Zhang, G. Ye, S. Soni, X. Qiu, T. L. Krijger, H. T. Jonkman, M. Carlotti, E. Sauter, M. Zharnikov and R. C. Chiechi, *Chem. Sci.*, 2018, **9**, 4414–4423.

42 V. Rabache, J. Chaste, P. Petit, M. L. Della Rocca, P. Martin, J. Lacroix, R. L. McCreery and P. Lafarge, *J. Am. Chem. Soc.*, 2013, **135**, 10218–10221.

43 R. Frisenda, V. A. E. C. Janssen, F. C. Grozema, H. S. J. van der Zant and N. Renaud, *Nat. Chem.*, 2016, **8**, 1099.

44 A. Kumar, N. Safdar, S. Kethireddy and D. Chateau, *Crit. Care Med.*, 2010, **8**, 1651–1664.

45 P. J. Stephens, F. J. Devlin, C. F. Chabalowski and M. J. Frisch, *J. Phys. Chem.*, 1994, **98**, 11623–11627.

46 J. P. Perdew, K. Burke and M. Ernzerhof, *Phys. Rev. Lett.*, 1996, **77**, 3865.

47 C. J. Judd, A. S. Nizovtsev, R. Plougmann, D. V. Kondratuk, H. L. Anderson, E. Besley and A. Saywell, *Phys. Rev. Lett.*, 2020, **125**, 206803.

48 A. D. Becke, *J. Chem. Phys.*, 1993, **98**, 5648–5652.

49 G. A. Petersson, A. Bennett, T. G. Tensfeldt, M. A. Al-Laham, W. A. Shirley and J. Mantzaris, *J. Chem. Phys.*, 1988, **89**, 2193–2198.

50 G. A. Petersson and M. A. Al-Laham, *J. Chem. Phys.*, 1991, **94**, 6081–6090.

51 R. Erich and E. K. U. Gross, *Phys. Rev. Lett.*, 1984, **52**, 997–1000.

52 J. Ferrer, C. J. Lambert, V. M. García-Suárez, D. Zs Manrique, D. Visontai, L. Oroszlany, R. Rodríguez-Ferradás, I. Grace, S. W. D. Bailey, K. Gillemot, H. Sadeghi and L. A. Algharagholy, *New J. Phys.*, 2014, **16**, 93029.

53 J. P. Perdew and Y. Wang, *Phys. Rev. B: Condens. Matter Mater. Phys.*, 1992, **45**, 13244.

54 E. Leary, B. Limburg, S. Sangtarash, A. Alanazy, I. Grace, K. Swada, L. J. Esdaile, M. M. Noori, T. González, G. Rubio-Bollinger, H. Sadeghi, N. Agrait, A. Hodgson, S. J. Higgins, C. J. Lambert, H. L. Anderson and R. Nichols, *J. Am. Chem. Soc.*, 2018, **140**, 12877–12883.

55 D. Zamel and A. U. Khan, *Inorg. Chem. Commun.*, 2021, **131**, 108766.

56 H. Kahlert, G. Meyer and A. Albrecht, *ChemTexts*, 2016, **2**, 1–28.

57 C. J. Lambert, *Quantum Transport in Nanostructures and Molecules*, IOP Publishing, Inc., Bristol, 2021, pp. 15–3.

58 C. J. Lambert and S. Liu, *Chem.–Eur. J.*, 2018, **24**, 4193–4201.

59 C. A. Coulson and G. S. Rushbrooke, *Math. Proc. Cambridge Philos. Soc.*, 1940, **36**, 193.

60 K. Yoshizawa, *Acc. Chem. Res.*, 2012, **45**, 1612–1621.

61 T. Tada and K. Yoshizawa, *Phys. Chem. Chem. Phys.*, 2015, **17**, 32099–32110.

62 Y. Tsuji and K. Yoshizawa, *J. Phys. Chem. C*, 2017, **121**, 9621–9626.

63 K. Okazawa, Y. Y. Tsuji and K. Yoshizawa, *J. Phys. Chem. C*, 2020, **124**, 3322–3331.

64 M. Camarasa-Gómez, D. Hernangómez-Pérez, M. S. G. Inkpen, E. Lovat, E. Fung, X. Roy, L. Venkataraman and F. Evers, *Nano Lett.*, 2020, **20**, 6381–6386.

65 O. A. Al-Owaedi, *ChemPhysChem*, 2024, **25**(1–12), e202300616.

66 A. Mochida, R. Nitta, A. Hashimoto and K. Matsui, *J. Jpn. Soc. Colour Mater.*, 2017, **90**, 97–101.

67 Z. Liu and T. Lu, *J. Phys. Chem. C*, 2020, **124**, 7353–7360.

68 H. A. Majeed and A. B. Sharba, *AIP Conf. Proc.*, 2022, **2547**, 030006.

69 G. Yang, J. Li, X. Deng, X. Song, M. Lu, Y. Zhu, Z. Yu, B. Xu, M. Li and L. Dang, *J. Phys. Chem. Lett.*, 2023, **14**, 6927–6934.

70 O. A. Al-Owaedi, *RSC Adv.*, 2024, **14**, 14704–14715.

71 O. Qi, P. Qian and S. Zhigang, *Nat. Commun.*, 2020, **11**, 4485.

72 A. V. Deshpande, A. Beidoun, A. Penzkofer and G. Wagenblast, *Chem. Phys.*, 1990, **142**, 123–131.

73 M. Büttiker and R. Landauer, *Phys. Rev. Lett.*, 1982, **49**, 1739–1742.

74 H. Quan, Z. KeJun, J. HuiLe, C. XiAn, H. MaoLin and W. Shun, *Sci. China: Chem.*, 2012, **55**, 1345–1350.

75 K. B. Male, E. Lam, J. Montes and J. H. T. Luong, *ACS Appl. Mater. Interfaces*, 2012, **4**, 3643–3649.

76 R. M. Al-Utayjawee and O. A. Al-Owaedi, *J. Phys.: Conf. Ser.*, 2021, **1818**, 12208.

77 M. Kamenetska, S. Y. Quek, A. C. Whalley, M. L. Steigerwald, H. J. Choi, S. G. Louie, C. Nuckolls, M. S. Hybertsen, J. B. Neaton and L. Venkataraman, *J. Am. Chem. Soc.*, 2010, **132**, 6817–6821.

78 S. Y. Quek, M. Kamenetska, M. L. Steigerwald, H. J. Choi, S. G. Louie, M. S. Hybertsen, J. B. Neaton and L. Venkataraman, *Nat. Nanotechnol.*, 2009, **4**, 230–234.

79 A. I. Yanson, G. R. Bollinger, H. E. van den Brom, N. Agrait and J. M. van Ruitenbeek, *Nature*, 1998, **395**, 783–785.

80 D. Xiang, X. Wang, C. Jia, T. Lee and X. Guo, *Chem. Rev.*, 2016, **116**, 4318–4440.

81 O. A. Al-Owaedi, T. T. Khalil, S. A. Karim, M. H. Said, E. Al-Bermany and D. N. Taha, *Syst. Rev. Pharm.*, 2020, **11**, 111–115.

82 R. Chen, I. Sharony and A. Nitzan, *J. Phys. Chem. Lett.*, 2020, **11**, 4261–4268.

83 C. Wu, D. Bates, S. Sangtarash, N. Ferri, A. Thomas, S. J. Higgins, C. M. Robertson, R. J. Nichols, H. Sadeghi and A. Vezzoli, *Nano Lett.*, 2020, **20**, 7980–7986.

84 R. Miao, H. Xu, M. Skripnik, L. Cui, K. Wang, K. G. L. Pedersen, M. Leijnse, F. Pauly, K. Wärnmark, E. Meyhofer, P. Reddy and H. Linke, *Nano Lett.*, 2018, **18**, 5666–5672.

85 D. Stefani, K. J. Weiland, M. Skripnik, C. Hsu, M. L. Perrin, M. Mayor, F. Pauly and H. S. J. van der Zant, *Nano Lett.*, 2018, **18**, 5981–5988.

86 L. O. Jones, M. A. Mosquera, B. Fu, G. C. Schatz, T. J. Marks and M. A. Ratner, *Nano Lett.*, 2019, **19**, 8956–8963.

87 J. R. Quinn, F. W. Foss, L. Venkataraman and R. Breslow, *J. Am. Chem. Soc.*, 2007, **129**, 12376–12377.

88 M. Taniguchi, M. Tsutsui, R. Mogi, T. Sugawara, Y. Tsuji, K. Yoshizawa and T. Kawai, *J. Am. Chem. Soc.*, 2011, **133**, 11426–11429.

89 B. Huang, X. Liu, Y. Yuan, Z. Hong, J. Zheng, L. Pei, Y. Shao, J. Li, X. Zhou, J. Chen, S. Jin and B. Mao, *J. Am. Chem. Soc.*, 2018, **140**, 17685–17690.

90 P. Moreno-Garcia, M. Gulcur, D. Z. Manrique, T. Pope, W. J. Hong, V. Kaliginedi, C. C. Huang, A. S. Batsanov, M. R. Bryce, C. J. Lambert and T. Wandlowski, *J. Am. Chem. Soc.*, 2013, **135**, 12228–12240.

91 B. Kim, J. M. Beebe, C. Olivier, S. Rigaut, D. Touchard, J. G. Kushmerick, X. Y. Zhu and C. D. Frisbie, *J. Phys. Chem. C*, 2007, **111**, 7521–7526.

92 Q. Lu, K. Liu, H. M. Zhang, Z. B. Du, X. H. Wang and F. S. Wang, *ACS Nano*, 2009, **3**, 3861–3868.

93 D. C. Milan, O. A. Al-Owaedi, M. Oerthel, S. Marqués-González, R. J. Brooke, M. R. Bryce, P. Cea, J. Ferrer, S. J. Higgins, C. J. Lambert, P. J. Low, D. Z. Manrique, S. Martin, R. J. Nichols, W. Schwarzacher and V. M. García-Suárez, *J. Phys. Chem. C*, 2016, **120**, 15666–15674.

94 M. H. Garner, H. X. Li, Y. Chen, T. A. Su, Z. Shangguan, D. W. Paley, T. F. Liu, F. Ng, H. X. Li, S. X. Xiao, C. Nuckolls, L. Venkataraman and G. C. Solomon, *Nature*, 2018, **558**, 415–419.

95 R. S. I. Mulliken, *J. Chem. Phys.*, 1955, **23**(35), 1833–1840.

96 B. A. A. Al-Mammory, O. A. Al-Owaedi and E. M. Al-Robayi, *J. Phys.: Conf. Ser.*, 2021, **1818**, 12095.

97 T. Markussen, M. Settness and K. S. Thygesen, *J. Chem. Phys.*, 2011, **135**, 144104.

98 M. Burkle, T. J. Hellmuth, F. Pauly and Y. Asai, *Phys. Rev. B: Condens. Matter Mater. Phys.*, 2015, **91**, 165419.

99 A. Putatunda and D. J. Singh, *Mater. Today Phys.*, 2019, **8**, 49–55.

100 N. T. Hung, A. R. T. Nugraha and R. Saito, *Energies*, 2019, **12**, 4561.

101 H. Ozawa, M. Baghernejad, O. A. Al-Owaedi, V. Kaliginedi, T. Nagashima, J. Ferrer, T. Wandlowski, V. M. García-Suárez, P. Broekmann, C. J. Lambert and M. Haga, *Chem.–Eur. J.*, 2016, **22**, 12732–12740.

102 F. Chen, X. Li, J. Hihath, Z. Huang and N. Tao, *J. Am. Chem. Soc.*, 2006, **128**, 15874–15881.

103 I. A. Shelykh, N. T. Bagraev and L. E. Klyachkin, *Semiconductors*, 2003, **37**, 1390–1399.

104 L. Cui, R. Miao, K. Wang, D. Thompson, L. A. Zotti, J. C. Cuevas, E. Meyhofer and P. Reddy, *Nat. Nanotechnol.*, 2018, **13**, 122–127.

105 W. Lee, K. Kim, W. Jeong, L. A. Zotti, F. Pauly, J. C. Cuevas and P. Reddy, *Nature*, 2013, **498**, 209–212.

106 H. B. Schlegel, J. S. Binkley and J. A. Pople, *J. Chem. Phys.*, 1984, **80**, 1976–1981.

107 C. J. Lambert, *Chem. Soc. Rev.*, 2015, **44**, 875–888.

108 B. Marius, J. H. Thomas, P. Fabian and A. Yoshihiro, *Phys. Rev. B: Condens. Matter Mater. Phys.*, 2015, **91**, 165419.

109 U. Sivan and Y. Imry, *Phys. Rev. B: Condens. Matter Mater. Phys.*, 1986, **33**, 551.

110 K. Esfarjani, M. Zebarjadi and Y. Kawazoe, *Phys. Rev. B: Condens. Matter Mater. Phys.*, 2006, **73**, 085406.

111 K. Müller, *J. Chem. Phys.*, 2008, **129**, 044708.

112 O. A. Al-Owaedi, *ACS Omega*, 2024, **9**, 10610–10620.

113 R. Davidson, O. A. Al-Owaedi, D. C. Milan, Q. Zeng, J. Tory, F. Hartl, S. J. Higgins, R. J. Nichols, C. J. Lambert and P. J. Low, *Inorg. Chem.*, 2016, **55**, 2691–2700.

114 R. J. Davidson, D. C. Milan, O. A. Al-Owaedi, A. K. Ismael, R. J. Nichols, S. J. Higgins, C. J. Lambert, D. S. Yufita and A. Beeby, *RSC Adv.*, 2018, **8**, 23585–23590.

115 S. Bock, O. A. Al-Owaedi, S. Eaves, D. C. Milan, M. Lemmer, B. Skelton, H. Osorio, R. Nichols, S. Higgins, P. Cea, N. Long, T. Albrecht, S. Martín, C. J. Lambert and P. J. Low, *Chem.–Eur. J.*, 2017, **23**, 2133–2143.